



This is the accepted manuscript made available via CHORUS, the article has been published as:

Polarization correlations for electron-impact excitation of the resonant transitions of Ne and Ar at low incident energies

L. R. Hargreaves, C. Campbell, M. A. Khakoo, J. W. McConkey, O. Zatsarinny, K. Bartschat, A. D. Stauffer, and R. P. McEachran

Phys. Rev. A **87**, 022711 — Published 25 February 2013

DOI: [10.1103/PhysRevA.87.022711](https://doi.org/10.1103/PhysRevA.87.022711)

Polarization correlations for electron impact excitation of the resonant transitions of Ne and Ar at low incident energies

L. R. Hargreaves, C. Campbell, M. A. Khakoo

Department of Physics, California State Fullerton, Fullerton, California 92831, USA

J. W. McConkey

Department of Physics, University of Windsor, Windsor, Ontario N9B 3P4, Canada

O. Zatsarinny, K. Bartschat

Department of Physics and Astronomy, Drake University, Des Moines, Iowa 50311, USA

A. D. Stauffer

Department of Physics and Astronomy, York University, Toronto, Ontario M3J 1P3, Canada

R. P. McEachran

Centre for Antimatter-Matter Studies, Research School of Physical Sciences and Engineering,
Australian National University, Canberra, ACT 0200, Australia

Abstract. The electron-polarized-photon coincidence method is used to determine linear and circular polarization correlations in the vacuum ultra-violet (VUV) for the differential electron impact excitation of neon and argon resonance transitions at impact energies of 25 eV and 30 eV at small scattering angles up to 40° . The circular polarization correlation is found to be positive in the case of Ne at 25 eV and supports the prediction of the present B-spline R-matrix theory concerning the violation of a long-established propensity rule regarding angular momentum transfer in electron impact excitation of $S \rightarrow P$ transitions. Comparisons with the results from the present Relativistic Distorted-Wave Approximation and an earlier Semi-Relativistic Distorted-Wave Born model are also made. For the case of Ar, at 25 eV and 30 eV, the circular polarization measurements remain in agreement with theory, but provide limited evidence to whether or not the circular polarization at small scattering angles is also positive. For the linear polarizations, much better agreement with theory is obtained than in earlier measurements carried out by Zheng and Becker (*Z. Phys. D* **23**, 137 (1992), *J. Phys. B* **26** 517 (1993)).

PACS number(s): 34.80.Bm, 34.80.Dp

1. Introduction

The application of electron-photon coincidence techniques in the measurement of electron-photon correlations has shed considerably more light on the dynamics of the scattering process regarding the differential electron impact excitation of atoms and molecules than conventional differential scattering experiments. Wide applications of this technique have been made since the pioneering work of Macek and Jaecks [1] on the theory of electron-photon correlations followed by the experimental study by Eminyan *et al.* [2]. Considerable progress has been made both theoretically and experimentally, as reviewed for example by Blum and Kleinpoppen [3], Andersen *et al.* [4], and Andersen and Bartschat [5] up to 2001. In the case of $S \rightarrow P$ excitations, the measurement of the circular polarization is important, as it is directly related to the angular momentum imparted to the target and hence gives insight into the dynamics of the collision process. In the VUV range this was first achieved by Khakoo *et al.* [6] using a double reflection, gold mirrors polarizer system [7] with He as the target and measuring the polarization correlation parameters for $1^1S \rightarrow 2^1P$ excitation in He. The experiment showed the reversal of the angular momentum transfer by the projectile electron, as compared to positive angular momentum transfer for small-angle scattering, around the scattering angle (θ) of 60° for the incident energy (E_0).

Until recently, extensive work on the orientation of atoms excited by electron impact strongly supported an empirical “propensity rule,” indicating that the sign of the angular momentum transfer, L_\perp , perpendicular to the scattering plane, is positive for $S \rightarrow P$ transitions at small scattering angles (θ), essentially independent of the projectile energy or the specific target [4]. Interest in the generality of this rule, and any physical basis for it, stems from the early work of Kohmoto and Fano [8], who considered a classical grazing-incidence collision from the attractive potential between the projectile electron and the target, which results in the excited state having a positive orbital angular momentum component perpendicular to the scattering plane. Further work on this problem was performed by Madison and

Winters [9], who pointed out a phase error in [8] and then analyzed the orientation in terms of the projectile charge in a perturbation series expansion. They predicted a difference in the sign of L_{\perp} between electron and positron impacts at small scattering angles, but without being able to predict the actual sign for either case. Andersen and Hertel [10] later developed a semi-classical model. While its validity was limited to small scattering angles, the model did offer the general prediction that the angular momentum transfer for electron-impact excitation processes was positive. Attempts to check the predictions of this model were made in a pioneering experiment reported by Shurgalin *et al.* [11], who studied electron scattering from the laser-excited 3p state in Na. Comparing de-excitation to the 3s ground state in super-elastic collisions with excitation to the 4s state in inelastic collisions, their results ultimately remained inconclusive for the 4s state. Bartschat *et al.* [12] explained the findings of Shurgalin *et al.* [11] by noting that the simple Andersen-Hertel model is not applicable to the Na (4s) case, due to the very large dipole polarizability of this state, which leads to an additional attractive potential that was neglected in the semi-classical argument.

Extensive compilations [4] of the available experimental data at the time, and many more theoretical predictions, showed the propensity for a positive angular momentum transfer at small scattering angles in $S \rightarrow P$ excitation to be seemingly very well fulfilled for the case of unpolarized incident electrons. An important generalization was presented by Andersen *et al.* [13], who analyzed the so-called generalized Stokes parameters [5,14] for a spin-polarized projectile beam. They found that parity conservation required the opposite sign of L_{\perp} for spin-up and spin-down (relative to the scattering plane) electrons for forward scattering. Once again, however, they noticed that the spin-averaged value in electron-impact excitation of the (6s6p) “ 3P_1 ” state in Hg fulfilled the propensity rule very well. This was also confirmed in an extensive compilation of data for spin-resolved electron impact [15]. The present measurements in Ne and Ar were instigated when recent theoretical results from the B-spline R-matrix (*BSR*) model showed that the propensity rule was violated for Ne in a restricted range of E_0 from

approximately 22 eV to 30 eV with the circular polarization P_3 ($= -L_{\perp}$, see below in section 2) reaching 0.14 at $E_0 = 25$ eV and $\theta = 30^\circ$ in a large 457-state *BSR* calculation (*BSR-457*).

In Ar, at $E_0 = 25$ eV and 30 eV, a similar trend was observed in smaller *BSR*-31 state calculations, i.e., the sign of P_3 was predicted positive below $\theta = 30^\circ$, however reaching a much smaller maximum (than in Ne) of 0.022 at $E_0 = 25$ eV and $\theta = 15^\circ$ and of 0.042 at $E_0 = 30$ eV and $\theta = 18^\circ$. While no P_3 measurements exist in the literature in this regime, linear polarization correlation measurements were carried out by Zheng and Becker [16,17]. Consequently, although the Ar case was significantly more challenging, we decided to undertake polarization correlation measurements also for Ar to see if we could provide experimental data for this target. At the same time, a much larger *BSR* model was set up, and we also decided to perform additional perturbative calculations using semi-relativistic and fully relativistic distorted-wave approaches. In this context, we also decided to independently test the data of Zheng and Becker [16,17], who reported significant disagreements with predictions by Bartschat and Madison [18]. This was somewhat surprising, since the measurements were performed in an angular range, where one would have expected the calculation to be fairly reliable.

2. General Theory

In the theory of angular and polarization correlation measurements, Andersen and Hertel [10] and Andersen *et al.* [4] defined the so-called coherence parameters, which reveal the details of the excitation in the most transparent way. These parameters are:

- (i) The alignment angle, γ , of the excited-state charge cloud relative to the incident electron direction.
- (ii) The linear polarization,

$$P_{lin} = (l - w) / (l + w), \quad (1)$$

where l and w define the relative length and width of the charge cloud in the scattering plane.

- (iii) The height parameter,

$$\rho_{oo} = h / (l + w + h), \quad (2)$$

where h is the relative height of the cloud perpendicular to the scattering plane; a nonzero value of ρ_{oo} is a direct indication of any spin-orbit coupling during the excitation.

(iv) The angular momentum, perpendicular to the scattering plane, L_{\perp} , transferred by the projectile electron to the orbital motion of the target electrons.

The present experiment is set up to measure polarization correlations (or normalized Stokes parameters) of the light emitted perpendicular to the scattering plane in coincidence with the scattered electron. It does not measure the ρ_{oo} parameter. However, it probes the positive reflection symmetry of the excited state with respect to this plane. The Stokes parameters are determined by measuring two linear (P_1, P_2) polarizations and one circular (P_3) polarization

$$P_1 = \eta_L \frac{I(0^\circ) - I(90^\circ)}{I(0^\circ) + I(90^\circ)}, \quad (3a)$$

$$P_2 = \eta_L \frac{I(45^\circ) - I(135^\circ)}{I(45^\circ) + I(135^\circ)} \quad (3b)$$

and

$$P_3 = \eta_C \frac{I(+)-I(-)}{I(+)+I(-)}, \quad (3c)$$

respectively, where $I(\alpha)$ is the coincidence signal for the polarizer set at the angle α with respect to the incident electron beam and $I(+)$, $I(-)$ are the polarizer setting for right- and left-handed circular polarized light, respectively (see Fig. 1 and details in section 3). Also, η_L and η_C are device dependent polarization efficiency factors for the measurement of linear and circular polarizations. Further,

$$P_{lin} = \sqrt{P_1^2 + P_2^2} \quad (4)$$

$$\tan 2\gamma = \frac{P_2}{P_1} \quad (5)$$

$$L_{\perp} = -P_3 \quad (6)$$

and,

$$P_{tot} = \sqrt{P_1^2 + P_2^2 + P_3^2} \leq 1. \quad (7)$$

In the fully coherent case the equality sign in (7) holds. The excitation is then completely specified by two parameters γ and L_{\perp} while $\rho_{oo} = 0$. Incoherence can manifest itself due to the addition of incoherent scattering processes (spin flips) or target effects such as hyperfine depolarization, spin-orbit interactions, etc. Then the inequality in (7) holds, in which case three parameters ($\gamma, P_{lin}, L_{\perp}$) must be used to specify the excitation, even if positive reflection symmetry still holds, since P_{lin} and L_{\perp} are now independent parameters. Positive reflection symmetry can be broken during the excitation process, e.g. by spin-flip processes, in which case the excited-state charge cloud acquires a finite height perpendicular to the scattering plane. To measure this ρ_{oo} height parameter requires a fourth Stokes parameter, P_4 , where the photon polarizer is placed in the scattering plane perpendicular to the incident electron. The relationship between P_4 and ρ_{oo} is (see [4]):

$$\rho_{oo} = \frac{(1+P_{lin})(1-P_4)}{4-(1-P_{lin})(1-P_4)}. \quad (8)$$

Andersen et al. [4] and Andersen and Bartschat [5] have discussed how – without any incoherence effects in the actual excitation process – further depolarization of the emitted radiation may take place due to fine- or hyperfine-structure effects during the time evolution of the decaying excited state.

3. Experiment

The setup of the experiment, shown in Fig. 1, is similar to that given in [19]. The apparatus consists of an electron energy-loss spectrometer and a VUV reflection polarizer, which is housed in a high-vacuum chamber made from stainless steel. The angular resolution of the spectrometer's electron

detection system was $\pm 2^\circ$, which is small, and appropriate for small θ work as is the case here. The chamber was evacuated by a ≈ 8 -in. turbo-molecular pump (Varian- TV 701 Navigator) providing an oil-free vacuum environment. Backing pump oil (low-grade diffusion pump oil; Difoil 20, K. J. Lesker Co.) was inhibited from streaming up the vacuum line into the pump by a micro-maze oil filter. The base pressure of the vacuum system was $\approx 1 \times 10^{-7}$ torr. Ne and Ar gas were delivered to the collision region via a 50-mm-long molybdenum needle of internal diameter 1 mm that was driven with a pressure of ≈ 0.35 torr. The needle was placed in the scattering plane perpendicular to the incident electron beam, so that it did not point into the photon polarizer. With the gas flowing, the vacuum chamber pressure rose to 5×10^{-7} torr. In this pressure regime, we expect radiation trapping to be negligible [19]. The electron spectrometer, described elsewhere [20], employed hemispherical energy selectors in the electron gun and analyzer regions and operated with a total energy resolution of 600 meV (full-width at half-maximum, FWHM) with an electron beam current between 1.0 and 1.5 μA . This energy resolution was insufficient to resolve the Ne ($2p^5[1/2]3s$) 1P_1 and ($2p^5[3/2]3s$) 3P_1 excited levels as well as the Ar ($3p^5[1/2]4s$) 1P_1 and ($3p^5[3/2]4s$) 3P_1 excited levels. Fortunately, the dominant triplet character of the 3P_1 states leads to a much smaller excitation cross-section compared to the 1P_1 state at an E_0 of 25 eV or 30 eV. Coupled with the much longer lifetime of the 3P_1 vs. the 1P_1 (21.0 ns versus 1.64 ns [21] for Ne and 8.5 ns versus 1.88 ns for Ar [22]), the coincident signal is expected to be relatively small at near forward scattering angles of this work. Quantitatively, using an experimental coincidence timing coincidence width of 10 ns (FWHM), for the triplet-singlet differential cross section ratio for Ne at $E_0=25$ eV [23], we estimate that the contribution of the 3P_1 state to the coincidence signal to be about 3% at $\theta=10^\circ$ about 5% at $\theta=40^\circ$, and therefore small. However, for Ar at $E_0=25$ eV, using the triplet-singlet differential cross section ratio from [24], we estimate that around $\theta=30^\circ$ the triplet contribution to the signal is about 20%, and at $E_0=30$ eV it is about 17%, and therefore small, but not negligible. However, for small-angle scattering theoretical models predict essentially the same coherence parameters for the

triplet and singlet states, so this should not affect our results here. VUV photons emitted from collision events were detected by a double reflection polarizer mounted perpendicular to the scattering plane. The principles of a reflection optics polarizer are well described in [7] and [16]. Here we will go briefly over some of the material covered in [7,16].

The polarizer, which viewed the collision region perpendicular to the scattering plane, consisted of two gold-plated mirrors (M1 and M2 in Fig. 1) that were flat to 1/10 of a wavelength (for $\lambda = 632$ nm, [25]) and whose normal vectors were mounted at incident (reflection) angles of $\theta_i = 57.5^\circ$ to the incident light. Linearly polarized light was measured by physically rotating M1 and M2 around the photon emission axis (angle α in Fig. 1), while holding M1 and M2 parallel to each other ($\phi_p = 0^\circ$ as illustrated in Fig. 1). To measure the circular polarization the polarizer was aligned at $\alpha = \pm 45^\circ$ to the major axis of the emitted radiation's polarization ellipse ($= \gamma$, from equations 3a, 3b and equation 5; see Fig. 1) while M2 was rotated to $\phi_p = \pm 45^\circ$ to behave as a quarter-wave plate [7]. The polarizer's linear and circular polarization efficiencies for all VUV transition lines of interest were determined from the experimental optical refractive index equations for the polarization efficiencies (η_L and η_C). This formulation is given in the Appendix. The detector was a channel electron multiplier (Detech Inc., model 203) with a 10 mm entrance outer diameter cone, which was coated with a double layer of CsI to enhance its quantum efficiency from its quoted value of about 10% without coating to approximately 23% for $\lambda=58.4$ nm and exceeding 60% for $\lambda>100$ nm [25]. We also note that the efficiency is also dependent on the polarization and angle of incidence [26,27], but assume that in this case for a cone-type geometry, this is averaged over and the detector should be essentially insensitive to polarization [27]. The entrance cone of the multiplier was biased at a negative voltage greater than E_0 to ground (our collision region is grounded) to repel electrons. Ions generated in the collision region do not generate counts even if they strike the multiplier, as their kinetic energies are well below 100 eV (if attracted to the multiplier) and in this case the quantum efficiency to generate secondary electrons is essentially zero.

The first reflector acts like a $\lambda/4$ plate in conventional transmission optics. At other wavelengths such as in the present work, the phase-shift deviates from 90° and thus a suitable correction must be made. The linear polarizations are determined using the device as a straightforward double linear polarization analyzer. Then γ of the charge cloud is determined using (5). Knowing the alignment of the polarization ellipse allows one to properly orient the polarization analyzer for the circular polarization measurements ϕ' which is given in [7] as

$$\tan 2\phi' = -\frac{P_1}{P_2} . \quad (9)$$

Comparison of (5) and (9) yields the relationship between ϕ' as defined above and γ , the alignment angle of the ellipse, as $\phi' = \gamma \pm 45^\circ$. The circular polarization is then obtained directly by measuring the coincidence rate at the two angular settings of ϕ' and measuring the coincidence rate with M2 (Fig. 1) set at the two positions $\pm 45^\circ$ about zero. Equation (A16) in Westerveld *et al.* [7] gives the normalized Stokes parameter (circular polarization) for a polarization-insensitive photon detector with the reflection phase difference between the parallel and perpendicular polarization incident light (Δ) in the second mirror assumed to be 90° and the first term in parentheses defining the polarization sensitivity of the device as negligible. In the case that Δ is not 90° a correction needs to be made with

$$P_3 = -\frac{1}{\cos 2\psi_r \sin 2\psi_r} \left[\frac{I(45^\circ, \phi') - I(-45^\circ, \phi')}{I(45^\circ, 0) + I(-45^\circ, 0)} \right] \pm P_{in} \cot(\Delta) . \quad (10)$$

The \pm sign in the $P_{in} \cot(\Delta)$ term in Eqn. (10) is taken as positive if $\phi' = \gamma - 45^\circ$ and negative if $\phi' = \gamma + 45^\circ$. The effects of finite angular acceptance of the polarizer can be determined by integration of incident ray paths (Gaussian acceptance optics) for this device. This variation was found to be about 2% for an acceptance angle of $\pm 3^\circ$ (FWHM) for the present device.

Test measurements of the electron impact coherent parameters for He ($\lambda = 58.4$ nm) were performed at an incident energy of $E_0 = 50$ eV, for the $(1s^2) ^1S \rightarrow (1s2p) ^1P$ transition in He, to ensure

the validity of our polarization efficiencies. The results were in very good agreement with the published data [4] and confirmed a positive L_{\perp} at small θ values, i.e., that our instrument was measuring the sign of the circular polarization correctly. Output pulses from the polarizer and electron spectrometer were processed using standard timing electronics. Time-coincident electron-photon events were recorded and analyzed by a data-acquisition computer, which also monitored the experiment and was responsible for setting and changing the position of the polarizer. LABVIEW™ custom data-acquisition software was developed in house for this study. Data-acquisition times per point ranged from two days to over two weeks, depending on the signal levels at each θ . Typical coincidence peak widths were in the region of 8-10 ns (full-widths at half maximum). The data taking sequence was as follows: at a fixed value of E_0 and θ , firstly P_1 and P_2 measurements were made with both mirrors parallel to each other, i.e. $\phi_p=0$ and, with the polarizer sequencing in between the polarization angle positions of $\alpha=-45^\circ, 0, 45^\circ, \pi$. At each position coincidence spectra were obtained with a dwell time of 600 seconds. Using the counts under each spectrum we deduced P_1 and P_2 from and Eqns. 3 and determined P_{lin} and γ from Eqns. 4 and 5. With the determination of γ , we then set the polarizer α angle at the alternating positions of $\alpha=\phi'=\gamma \pm 45^\circ$. In each of these alternating positions, M2 was rotated to $\phi_p=\pm 45^\circ$. The four coincidence spectra at the two α values and two ϕ_p values (dwell time at each was 600s) were used to determine P_3 from Eqn. (10) using the P_{lin} values at this angle. The two values of P_3 obtained were averaged to produce the final value of P_3 . A typical value for the $P_{lin} \cot(\Delta)$ correction term in Eqn. (10) was around 0.1; this is not negligible and adds to our errors.

We also note that the polarization values had to be corrected for polarization efficiencies of the linear and circular polarization modes (Table A-1). In this experiment the polarization efficiency for the polarizer in the linear polarization mode (η_L) was calculated using the refractive index (n) and extinction coefficient (k) data from [28] for gold at the appropriate wavelengths (λ), but further corrected by

measuring the non-coincidence polarized radiation emitted by He as measured by Mumma *et al.* [29] $E_0=50$ eV and 80 eV. Unfortunately for the circular polarization efficiency (η_C) there was no readily available calibration standard, and consequently only theoretical values of η_C were used as given in Table A-1.

4. Theoretical Methods

4a. Relativistic Distorted-Wave (RDW) Approximation

The Relativistic Distorted-Wave (RDW) approximation [30] is based on solutions of the Dirac equations for the wave functions for both the bound atomic states and the scattered electron. The ground and excited atomic state wave functions were calculated separately using the Multi-Channel Dirac-Fock program [31]. The ground state was represented in j - j coupling by a single configuration $n\bar{p}^2np^4$ while the excited state was a linear combination of the configurations $n\bar{p}^2np^3(n+1)s$ and $n\bar{p}np^4(n+1)s$ where \bar{p} represents a p-electron with total angular momentum $j = 1/2$ and p represents a p-electron with $j = 3/2$ while $n = 2$ for Ne and $n = 3$ for Ar. For the excited state the configurations were coupled to a total angular momentum $J = 1$.

The distorted wave in the incident channel was a solution of the Dirac equations including the static potential of the ground state while in the excited channel it was calculated using the spherically-symmetrized static potential of the excited state. Using these wave functions, the scattering amplitudes were calculated and the various Stokes parameters evaluated using the formulae of [4].

4b. Semi-Relativistic Distorted-Wave Approximation (DWBA)

In order to show the theoretical developments of the past 25 years, we present predictions from the DWBA calculations published by Bartschat and Madison [18] in 1987. They used target wave functions generated by the *SUPERSTRUCTURE* code [32]. For the calculations of the distorted waves, the static

potential generated from these wave functions was supplemented by local potentials to simulate the effects of electron exchange, the polarization of the charge cloud due to the incident electron, and loss of flux into inelastic channels. Relativistic effects were also accounted for in the calculation of the distorted waves through additional correction terms in the distortion potential.

4c. Breit-Pauli B-Spline R-Matrix (*BSR*) with Pseudo-States Approach

With the rapidly increasing computational power over the past years, much algorithm development has concentrated on fully *ab initio*, nonperturbative methods for the description of atomic collision processes. One of such approaches is the B-Spline R-Matrix (*BSR*) method [33]. It represents an alternative to the well-known Belfast suite of R-Matrix codes [34] to solve the close-coupling equations, with several key modifications that have proven to be particularly advantageous for complex targets. The distinctive feature of the method is the use of B-splines as a universal basis to represent the scattering orbitals in the inner region of the R-matrix box. Furthermore, employing individually optimized, and hence nonorthogonal sets of one-electron radial functions for the target states provides high flexibility and accuracy in the structure description. Finally, we are now in a position to include a large number of pseudo-states in the close-coupling expansion in order to simulate the effect of coupling to the high-lying Rydberg states and, most importantly, to the ionization continuum using the general R-matrix with pseudo-states (*RMPS*) [35] philosophy.

For the present work specifically, we set up a close-coupling expansion including 457 target states for e-Ne collisions, with the lowest 87 states representing the bound spectrum and the remaining 370 the ionization continuum. More details about this calculation can be found in [36]. The corresponding *RMPS* model for e-Ar contained a total of 500 states, 78 for the bound spectrum and 422 for the continuum. While a fully relativistic version of the *BSR* complex exists [37], we chose to perform semirelativistic calculations by including the one-electron terms of the Breit-Pauli Hamiltonian in setting up the matrices. The size of these matrices (currently up to 120,000), which need to be diagonalized for

the inner region, would be doubled in a fully relativistic approach. This is computationally prohibitive at the current time. Fortunately, neutral Ne and Ar are targets for which a Breit-Pauli approach is expected to be sufficient. Remaining discrepancies between experiment and theory are most likely due to reasons other than the treatment of relativistic effects.

5. Results and Discussion

Table 1 shows a summary of our experimental results. Figure 2 exhibits our polarization correlation parameters for Ne at $E_0 = 25$ eV, which were also reported in [38]. For the linear polarization parameters, the *DWBA* [29] and the present *BSR* and *RDW* models show excellent agreement with each other as well as with the present experiment, which is restricted by statistics to $\theta < 40^\circ$. The models diverge from each other for $\theta > 60^\circ$. Both the *DWBA* and *RDW* are intermediate-energy models and the fact that they are in good agreement in the experimental range is very encouraging. In particular, agreement between theory and experiment in the value of γ , which is used to locate the experimental position of the polarizer for the measurement of P_3 is excellent. We also note that the experimental value of the P_{lin} parameter is in general close to 1, albeit below by about 6% on average. Our error bars, however, are too large to make a precise deduction, and we could likely also have a small systematic error due to our determination of η_L and η_C to compound this issue.

The above results can be qualitatively understood by recalling the results of the first-order plane-wave Born approximation (*PWBA*). The *PWBA* predicts $P_{lin} = 1$ and the alignment angle γ to be the angle of the momentum-transfer direction [4,5]. In other words, if the *PWBA* is a reasonable approximation, then the linear polarizations depend only on the scattering angle and the energy loss – they are *completely independent of the numerical model*.

For the $P_3 (= -L_\perp)$ parameter in Ne, the models show severe disagreement. The present experiment shows very good agreement with the *BSR* predictions for Ne, which motivated this project. As reported in [38], the *BSR* only predicts positive P_3 values if it includes channels exceeding the minimum 5-state model (the $2p^6$ ground state plus the four fine structure states of the $2p^53s$ configuration). Such channel-coupling is not prevalent in the *DWBA*, which shows the usual P_3 form predicted by [8], although the drop in P_3 from zero is less dramatic than what is usually observed at higher E_0 values. The *BSR* theory also predicts P_3 to become negative around $\theta = 43^\circ$ and then to change sign around $\theta = 75^\circ$, a pattern that is usually observed for He and the other rare gases. We also note that the *BSR* model predicts a very large (0.995) positive P_3 value around $\theta = 94^\circ$. For our P_{tot} parameter, hyperfine depolarization is expected to be negligible (Ne has only a 0.257% odd atomic weight isotope [39]). Theory predicts values of essentially unity, in good agreement with the present experimental work, albeit with large error bars. Although not shown here, we note that the *RDW* values for P_3 at small θ change rapidly for $E_0 < 25$ eV. In fact, the *RDW* results for P_3 become positive at $E_0 = 20$ eV for small $\theta \leq 30^\circ$. These latter findings, as well as the *DWBA* results for Ar shown below, suggest that *channel coupling alone is not responsible* for the unusual small-angle P_3 values at certain energies. Recall that the *PWBA* predicts $P_3 = 0$ for all energies and angles [4,5]. In other words, any more sophisticated model than the *PWBA* will deviate from the zero value. Apparently, already the direction of this deviation can be very sensitive to the collision energy and the details of the model. The more sophisticated models will, of course, also predict deviations of P_{lin} and P_{tot} from unity. However, these deviations will be small, even for P_3 values of 20%, due to the mathematical relations outlined above. Consequently, such deviations are very difficult to confirm experimentally, and the same is true for deviations of γ from the momentum-transfer direction.

In Figs. 3 and 4, our linear polarization correlation measurements for Ar are compared with earlier experimental work (linear polarization parameters only) by Zhang and Becker [16,17] and with the *DWBA*, *RDW* and present *BSR* models. As in Ne, all three theories (*DWBA*, *RDW* and *BSR*) show excellent agreement with each other up to $\theta \approx 50^\circ$ and also with the present experimental data, which are again restricted by statistics to θ up to 30° . Referring back to the discussion above, this good agreement is ultimately not very surprising, since the *PWBA* can be expected to be a reasonable model in the small-angle regime. Consequently, it is not clear why the earlier experimental data of [16,17] deviated so much from these predictions. In these figures, comparison of P_3 values for Ar shows a mixed picture. At $E_0 = 25$ eV, the experimental P_3 value is essentially zero, more in agreement with the *DWBA* than the *BSR* or the *RDW* which are in good agreement with each other. This is, however, not the result of the influence of the “ 3P ” component which, as mentioned above, since from the *BSR* model the P_3 value for the “ 3P ” state of Ar is also negative at small θ at both 25 eV and 30 eV.

In fact, all theories predict very similar results for the physical singlet and triplet states at the small angles covered by the experiment. This is due to the fact that these states can be well described in an intermediate-coupling scheme as linear combinations of *LS*-coupled singlet and triplet states [40]. Even though the singlet admixture is smaller in the physical triplet state than in its singlet counterpart, the excitation at small angles is effectively determined by this component. The triplet admixture, and hence exchange scattering and the possible spin-flips associated with it, is basically negligible.

The result for Ar at 25 eV may need to be independently checked. At $E_0 = 30$ eV, the experimental P_3 values are in the negative range in agreement with all theories, but unfortunately with large error bars that do not provide a stand-alone data set or a robust test of these models. The experiment, however, coupled with the predictions of the models, supports the fact that the P_3 values for Ar are negative at small θ . Hence the overall picture regarding the small θ P_3 values suggests that positive P_3 values at

small θ seem to be unique to Ne over a restricted range of E_0 values around 20–25 eV. Since, based on the discussion above, L_{\perp} studied for the targets, energies, and angles in the present work is *orbital angular momentum orientation of the singlet part of the wave function*, it is unlikely that semi-classical arguments will be able to explain the deviations from the propensity rule. We believe that these deviations are associated with quantum mechanical interference effects.

6. Summary and Conclusions

We have observed exceptions to the propensity rule of a positive angular momentum transfer in the electron impact excitation of an $S \rightarrow P$ transition at small scattering angles for excitation of the resonance transition in Ne at 25 eV, as predicted by a large *BSR* model. This prediction is also supported by our *RDW* model at $E_0 = 20$ eV for Ne, but we have not yet verified it experimentally at this energy. The positive P_3 values from theory are well supported by our experiment for Ne at $E_0 = 25$ eV. Positive deviations of the P_3 values could not be verified experimentally for Ar on account of the larger error bars and the considerably smaller absolute P_3 values in Ar as compared to Ne. At 30 eV the small-angle P_3 values in Ar from experiment and theory are negative. Interestingly, only the *DWBA* model predicted positive small-angle P_3 values for Ar at 25 eV. In general, the effect seems to be limited to a small window of energies of around 20 – 30 eV for these targets. It would be of interest to investigate this issue also in Kr and Xe. If violations of the propensity rules do occur in these targets, this might provide further insight into the scattering dynamics and serve as a sensitive test of theoretical models. More studies would also be helpful to further test present theoretical models and challenge experimental methods for polarization correlation measurements. Given the apparent validity of the *PWBA* predictions at small angles for all but the circular polarization, measurements in this angular range should concentrate on P_3 , with the linear polarizations mostly serving as a consistency check rather than

a test of a particular theoretical model. In order to perform a test of theory beyond P_3 , the experiments would need to be performed over a much wider angular range.

7. Acknowledgments

This work was supported, in part, by the United States National Science Foundation under Grant No. RUI-PHY-0965793 (LRH, CC, MAK), No. PHY-1212450 (OZ and KB), and No. PHY-1068140 (KB). ADS and JWM are grateful for financial support from NSERC Canada.

8. Appendix

Reflection Polarizer Parameters.

The η_L and η_C are polarization efficiency factors, used in equations 3, were determined from the experimental optical refractive index n and extinction values k of the gold mirrors [28], using the appropriate formulas given in [26]. We note here that similar formulae are given in a similar, but later publication [41], with severe typographic errors. This is another reason why we carefully list these formulae here.

Using n, k we define parameters a, b ,

$$2a^2 = [(n^2 - k^2 - \sin^2 \theta_i)^2 + 4n^2 k^2]^{1/2} + (n^2 - k^2 - \sin^2 \theta_i) \quad (\text{A-1})$$

$$2b^2 = [(n^2 - k^2 - \sin^2 \theta_i)^2 + 4n^2 k^2]^{1/2} - (n^2 - k^2 - \sin^2 \theta_i), \quad (\text{A-2})$$

where θ_i is the angle of incidence of the light on the mirror, from which the reflection coefficients parallel (R_s) and perpendicular (R_p) to the plane of the gold mirror can be derived (see [21]):

$$R_s = \frac{a^2 + b^2 - 2a \cos \theta_i + \cos^2 \theta_i}{a^2 + b^2 + 2a \cos \theta_i + \cos^2 \theta_i} = \frac{(a - \cos \theta_i)^2 + b^2}{(a + \cos \theta_i)^2 + b^2} \quad (\text{A-3})$$

$$R_p = R_s \frac{a^2 + b^2 - 2a \sin \theta_i \tan \theta_i + \sin^2 \theta_i \tan^2 \theta_i}{a^2 + b^2 + 2a \sin \theta_i \tan \theta_i + \sin^2 \theta_i \tan^2 \theta_i} = R_s \frac{(a - \sin \theta_i \tan \theta_i)^2 + b^2}{(a + \sin \theta_i \tan \theta_i)^2 + b^2}. \quad (\text{A-4})$$

Following this, the single mirror linear polarization efficiency is

$$\eta_{1L} = \frac{R_S - R_P}{R_S + R_P} = \frac{1}{\cos 2\Psi_R}, \quad (\text{A-5})$$

and the double mirror linear polarization efficiency equals [7]

$$\eta_{2L} = \eta_L = \frac{1 + \cos^2 2\Psi_R}{2 \cos 2\Psi_R}. \quad (\text{A-6})$$

The phase-shift Δ_P , Δ_S of the perpendicular and parallel polarization components of the light are respectively,

$$\tan \Delta_P = \frac{2b \cos \theta_i + a^2 + b^2 - \sin^2 \theta_i}{(a^2 - b^2) - [a^2 - b^2 + \sin^2 \theta_i]^2 + 4a^2 b^2} \cos^2 \theta_i = \frac{A}{B}, \quad (\text{A-8})$$

$$\tan \Delta_S = \frac{-2b \cos \theta_i}{a^2 - b^2 - \cos^2 \theta_i} = \frac{A'}{B'}, \quad (\text{A-9})$$

and the phase difference between the two components is

$$\Delta = \Delta_P - \Delta_S = \tan^{-1} \left(\frac{A}{B} \right) - \tan^{-1} \left(\frac{A'}{B'} \right). \quad (\text{A-10})$$

Finally, the circular polarization efficiency for the double reflection polarizer is,

$$\eta_{2C} = \eta_C = \frac{-1}{\cos 2\Psi_R \sin 2\Psi_R \sin \Delta}. \quad (\text{A-11})$$

Finally, Table A-1 gives n , k and Δ for gold at several VUV wavelengths.

9. References

- [1] J. Macek and D. Jaecks, Phys. Rev. A **4**, 2288 (1971).
- [2] M. Eminyan, K. B. MacAdam, J. Slevin, and H. Kleinpoppen, Phys. Rev. Lett. **31** 576 (1973).
- [3] K. Blum and H. Kleinpoppen, Phys. Rep. **52**, 203 (1979).
- [4] N. Andersen, J. W. Gallagher, and I. V. Hertel, Phys. Rep. **165**, 1 (1988).
- [5] N. Andersen and K. Bartschat, *Polarization, Alignment, and Orientation in Atomic Collisions* (Springer-Verlag, New York, 2001).
- [6] M. A. Khakoo, J. L. Forand, K. Becker, and J. W. McConkey, J. Phys. B **19**, L209-213 (1986).
- [7] W. B. Westerveld, K. Becker, P. W. Zetner, J. J. Corr, and J. W. McConkey, Appl. Opt. **24** 2256-62 (1985).
- [8] M. Kohmoto and U. Fano, J. Phys. B **14**, L447 (1981).
- [9] D. H. Madison and K. H. Winters, Phys. Rev. Lett. **47**, 1885 (1981).
- [10] N. Andersen and I. V. Hertel, Comments At. Mol. Phys. **19**, 1 (1986).
- [11] M. Shurgalin, A. J. Murray, W. R. MacGillivray, M.C. Standage, D. H. Madison, K. D. Winkler, and I. Bray, Phys. Rev. Lett. **81**, 4604 (1998).
- [12] K. Bartschat, N. Andersen, and D. Loveall, Phys. Rev. Lett. **83**, 5254 (1999).
- [13] N. Andersen, K. Bartschat, J. T. Broad, G. F. Hanne, and M. Uhrig, Phys. Rev. Lett. **76**, 208 (1996).
- [14] N. Andersen and K. Bartschat, J. Phys. B **27**, 3189 (1994); **29**, 1149 (1996).
- [15] N. Andersen, K. Bartschat, J. T. Broad, and I. V. Hertel, Phys. Rep. **279**, 251 (1997).
- [16] S. H. Zheng and K. Becker, J. Phys. B **26** 517 (1993).
- [17] S. H. Zheng and K. Becker, Z. Phys. D **23**, 137 (1992).
- [18] K. Bartschat and D. H. Madison, J. Phys. Rep. **20**, 5839 (1987).

- [19] M. A. Khakoo and J. W. McConkey, *J. Phys. B* **20**, 554 (1987).
- [20] K. E. James Jr., J. G. Childers, and M. A. Khakoo, *Phys. Rev. A* **69**, 022710 (2004).
- [21] [<http://physics.nist.gov/cgi-bin/ASD/lines1.pl>].
- [22] W. C. Martin and W. L. Wiese, *Atomic Spectroscopy, in Springer Handbook of Atomic, Molecular, and Optical Physics, Part B*, Ch. 10, 175-198 (Edited by G. W. F. Drake, Springer Science and Business Media, Inc., New York) (2006).
- [23] M. A. Khakoo, J. Wrkich, M. Larsen, G. Kleiban, I. Kanik, S. Trajmar, M. J. Brunger, P. J. O. Teubner, A. Crowe, C. J. Fontes, R. E. H. Clark, V. Zeman, K. Bartschat, D. H. Madison, R. Srivastava and A. D. Stauffer, *Phys. Rev. A* **65**, 062711 (2002).
- [24] M. A. Khakoo, P. Vandeventer, J. G. Childers, I. Kanik, C. J. Fontes, K. Bartschat, V. Zeman, D. H. Madison, S. Saxena, R. Srivastava and A. D. Stauffer, *J. Phys. B* **37**, 247 (2003).
- [25] Edmund Optics, Barrington, New Jersey 08007, USA, model NT01-913-566.
- [26] J. A. R. Samson, *Techniques of Vacuum Ultraviolet Spectroscopy*, (Pied Publications, Lincoln, Nebraska, 1967).
- [27] J. Tome, P. Zetner, W. B. Westerveld, and J. W. McConkey, *App. Optics* **23** 656 (1984).
- [28] D. W. Lynch and W. R. Hunter, in *Handbook of Optical Constants of Solids*, (Academic Press, Orlando Florida, 1985), Editor: E. D. Palik.
- [29] M. J. Mumma, M. Misakian, W. M. Jackson, and J. L. Faris, *Phys. Rev. A* **9**, 203 (1974).
- [30] T. Zuo, R. P. McEachran, and A. D. Stauffer, *J. Phys. B* **24**, 2853 (1991).
- [31] I. P. Grant, B. J. McKenzie, P. H. Norrington, D. F. Mayers, and N. C. Pyper, *Comp. Phys. Comm.* **21**, 207 (1980).
- [32] W. Eissner, M. Jones, and H. Nussbaumer, *Comp. Phys. Commun.* **8**, 270 (1974).
- [33] O. Zatsarinny, *Comp. Phys. Commun.* **174**, 273 (2006).
- [34] K. A. Berrington, W. B. Eissner, and P. H. Norrington, *Comp. Phys. Commun.* **92**, 290 (1995).

- [35] K. Bartschat, E. T. Hudson, M. P. Scott, P. G. Burke and V. M. Burke, *J. Phys. B* **29**, 115 (1996).
- [36] O. Zatsarinny and K. Bartschat, *Phys. Rev. A* **86**, 022717 (2012).
- [37] O. Zatsarinny and K. Bartschat, *Phys. Rev. A* **77**, 062701 (2008).
- [38] L. R. Hargreaves, C. Campbell, and M. A. Khakoo, O. Zatsarinny, and K. Bartschat, *Phys. Rev. A* **85**, 050701(R) (2012).
- [39] J. J. Corr, P. J. M. van der Burgt, P. Plessis, M. A. Khakoo, P. Hammond, and J. W. McConkey, *J. Phys. B* **24**, 1069 (1991).
- [40] K. Bartschat and D. H. Madison, *J. Phys. B* **25** 4619 (1992).
- [41] J. A. R. Samson and D. L. Ederer, *Vacuum Ultraviolet Spectroscopy I, Experimental Methods in the Physical Sciences* (Academic Press, San Diego, California, 2000) Editors: L. Marton and C. Marton.

θ (deg)	P_1	Error	P_2	Error	P_3	Error	P_{lin}	Error	γ (deg)	Error	P_{tot}	Error
Ne 25eV												
10	0.85	0.05	-0.37	0.05	0.04	0.11	0.93	0.06	-11.6	1.5	0.97	0.06
15	0.66	0.09	-0.54	0.09	0.24	0.12	0.86	0.09	-19.7	3.0	0.90	0.10
20	0.47	0.07	-0.67	0.07	0.22	0.12	0.82	0.07	-27.5	2.4	0.83	0.07
25	0.30	0.12	-0.94	0.08	0.18	0.10	0.91	0.11	-35.3	3.7	0.91	0.11
30	0.093	0.069	-0.91	0.09	0.25	0.11	0.93	0.09	-41.2	3.0	0.95	0.14
40	-0.29	0.11	-0.82	0.14	0.02	0.17	0.87	0.14	-54.7	3.9	0.87	0.14
Ar 25eV												
10	0.00	0.12	-0.98	0.17	0.04	0.12	0.99	0.18	-45.1	3.5	1.02	0.21
15	-0.31	0.13	-0.83	0.17	0.14	0.17	0.89	0.16	-55.2	4.3	0.90	0.16
20	-0.80	0.15	-0.18	0.13	0.00	0.26	0.82	0.15	-83.8	4.6	0.82	0.15
25	-0.67	0.16	0.42	0.13	0.03	0.2	0.80	0.15	74.0	5.0	0.79	0.16
Ar 30eV												
10	0.19	0.09	-0.99	0.14	0.13	0.09	1.00	0.13	-39.6	2.5	1.01	0.13
15	-0.68	0.11	-0.61	0.10	-0.06	0.12	0.90	0.16	-69.1	3.3	0.91	0.18
20	-0.96	0.18	0.16	0.10	-0.10	0.14	0.97	0.18	85.3	3.2	0.98	0.19
25	-0.79	0.18	0.70	0.11	-0.22	0.14	1.03	0.15	68.5	4.0	1.06	0.15
30	0.25	0.14	0.77	0.14	-0.16	0.14	0.81	0.14	36.0	4.8	0.83	0.14

Table 1. Polarization correlation parameters for the resonance transitions in Ne and Ar. Error bars are one standard deviation.

Species	Energy (eV)	λ (nm)	n	k	$\cos(2\Psi_R)$	$\sin(2\Psi_R)$	η_{1L}	η_{2L}	Δ (deg)	η_{2C}
He	21.218	58.4	1.069	0.838	0.6440	0.7650	1.5528	1.0361	91.1	-2.03
Ne	16.848	73.6	1.040	0.694	0.6763	0.7366	1.4787	1.0775	82.6	-2.02
Ar	11.828	104.8	1.216	0.864	0.7077	0.7065	1.4130	1.0604	97.4	-2.02
Kr	10.644	116.5	1.244	0.939	0.6930	0.7209	1.4430	1.0680	101.4	-2.04
Kr	10.033	123.6	1.278	0.985	0.6890	0.7248	1.4515	1.0702	104.3	-2.07
Xe	9.570	129.6	1.306	1.019	0.6862	0.7274	1.4573	1.0718	106.5	-2.09
Xe	8.437	147.0	1.400	1.097	0.6851	0.7284	1.4595	1.0723	112.1	-2.16

Table A-1. Refractive index, extinction coefficients, and polarization parameters (see equations A1-A11) for radiation reflection by gold at selected resonant VUV wavelengths incident at the angle of 57.5° .

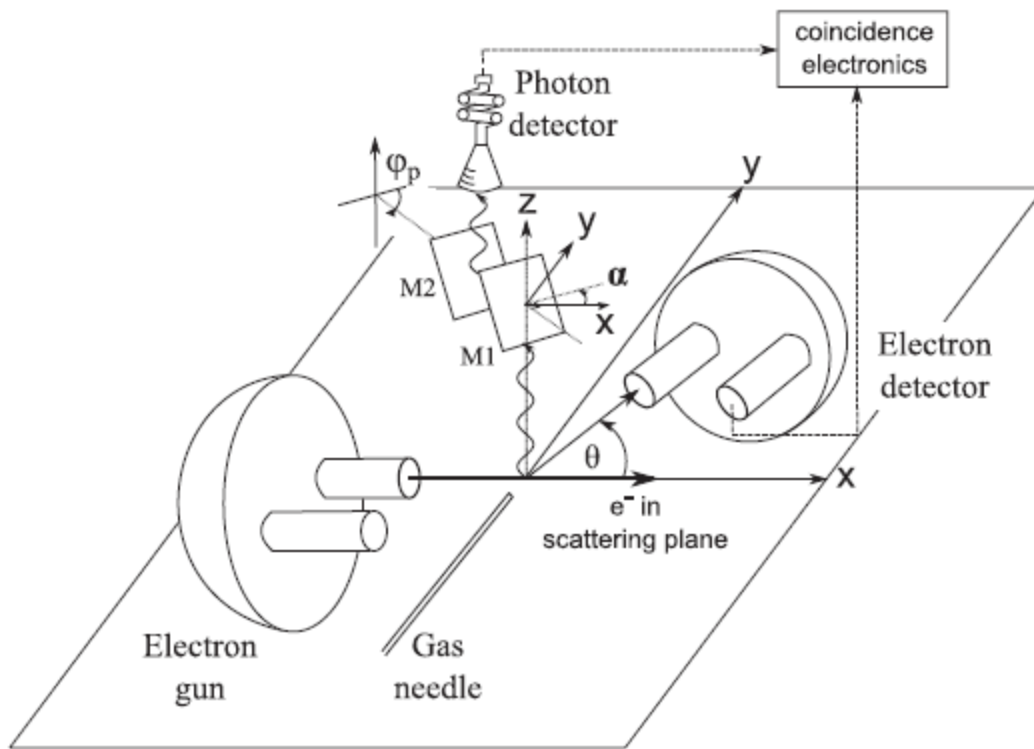


Figure 1: Schematic diagram of the experimental setup. Note that $\phi_p = 0^\circ$ for the arrangement of M1 and M2 shown. See text for details.

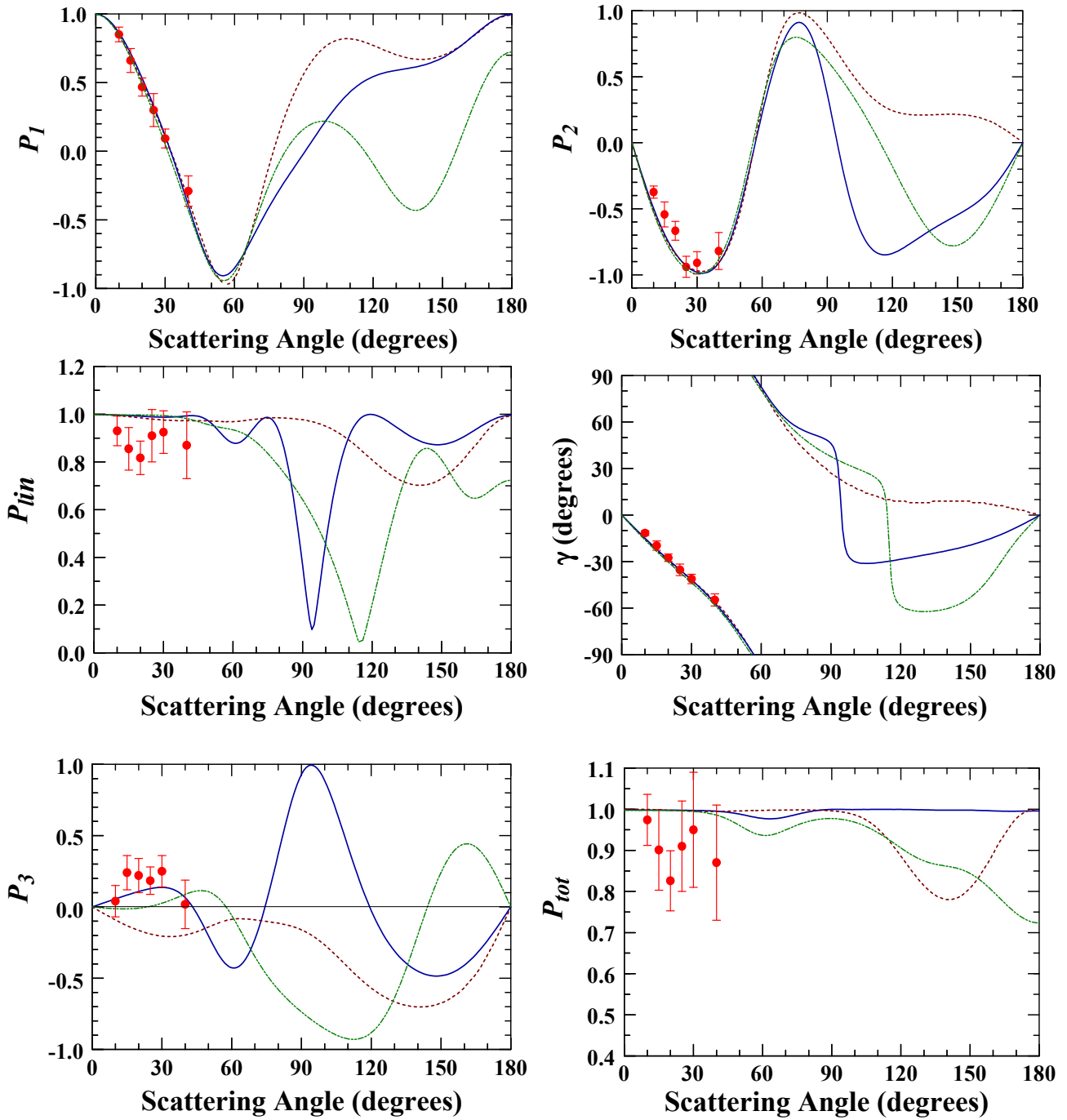


Figure 2 (color online): Polarization correlation parameters for Ne at $E_0 = 25$ eV. Legend: \bullet Present experiment with one standard deviation error bars; $—$ (blue) *BSR-457* model; $- -$ (green) *RDW*; $- -$ (brown) *DWBA* [18]. See text for details and discussion.

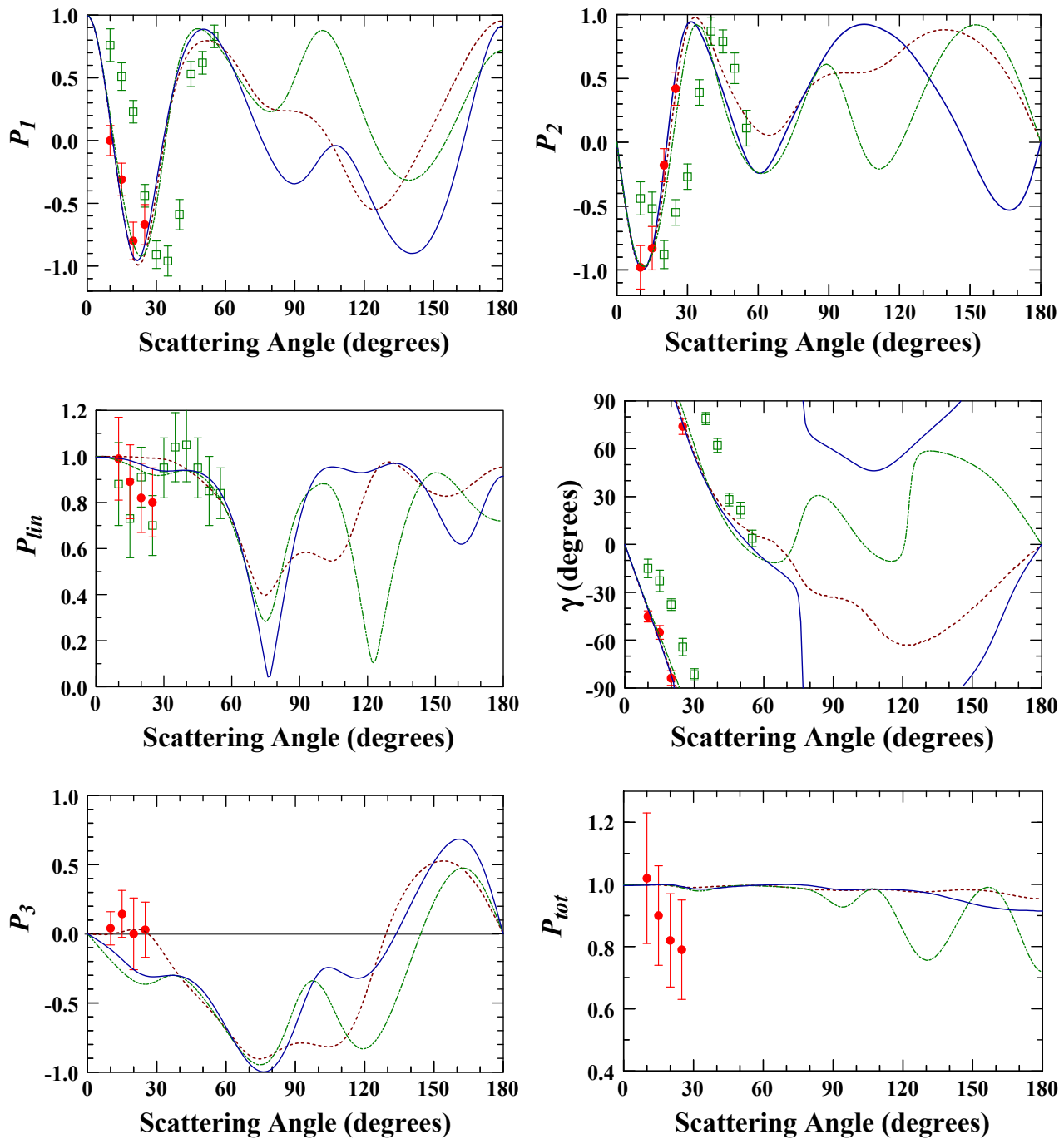


Figure 3 (color online): Polarization correlation parameters for Ar at $E_0 = 25$ eV. Legend is the same as Fig. 2 except for: — $BSR-500$ model; experiment: \square Zheng and Becker [16]. See text for discussion.

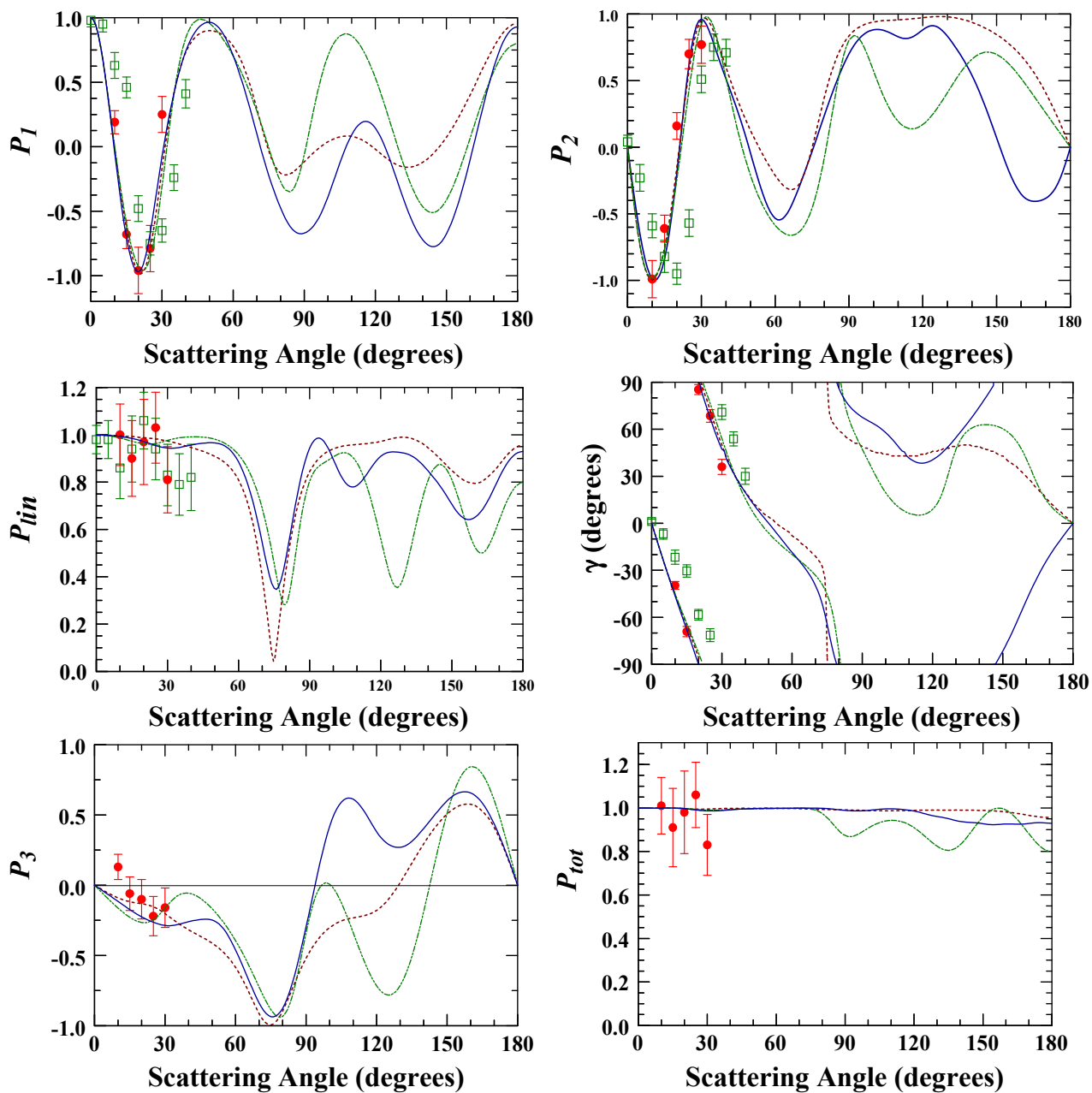


Figure 4 (color online): Polarization correlation parameters for Ar at $E_0 = 30$ eV. Legend is the same as Fig. 3 except for: experiment: \square Zheng and Becker [17].